Contribution from the Laboratoire de Chimie de Coordination, UA au CNRS No. 1194, Laboratoires de Chimie, Département de Recherche Fondamentale, and Service de Physique/Structure, Département de Recherche Fondamentale, Centre d'Etudes Nucléaires de Grenoble, 85X, F-38041 Grenoble Cedex, France, Laboratoire de Chimie Théorique, UA au CNRS No. 510, Université de Nancy-I, B.P. 239, F-54506 Vandoeuvre-les-Nancy, France, and LURE, Laboratoire Propre du CNRS, CEA & MEN, Université de Paris-Sud/Orsay, Bâtiment 209 D, F-91405 Orsay Cedex, France

trans-Dihalogenotitanium(IV) Porphyrins, Cis-Disubstituted Analogues, and Titanium(III) Derivatives. Characterization and Structural Investigations Combining X-ray Crystallography and Difference EXAFS Spectroscopy

Jean-Claude Marchon,*[†] Jean-Marc Latour,[†] André Grand,[†] Michel Belakhovsky,[‡] Michel Loos,[§] and José Goulon*[§,∥,⊥]

Received February 1, 1989

Dihalogenotitanium(IV) tetraphenylporphyrins [(TPP)$Ti^{IV}X_2$] and octaethylporphyrins [(OEP)$Ti^{IV}X_2$] were prepared by reaction of the appropriate hydrogen halide HX (X = F, Cl, Br) with the parent oxotitanium(IV) complex. Similarly, the reaction of the titanyl porphyrin complexes with catechol or 3,4-toluenedithiol afforded cis-disubstituted derivatives: [(TPP)$Ti^{IV}(-O-)_2$Ph] (**5**) and [(TPP)$Ti^{IV}(-S-)_2$Tol] (**6**). Zinc amalgam reduction of [(TPP)$Ti^{IV}F_2$] (**2**) yielded the mononuclear titanium(III) complex [(TPP)Ti^{III}F] (**7**), whereas the anionic species [(TPP)$Ti^{III}F_2]^-$ (**8**) was prepared by electrochemical reduction of **2** or by fluoride addition to **7**. The structure of **2** was determined by single-crystal X-ray diffraction: [(TPP)$Ti^{IV}F_2$] crystallizes in the tetragonal $I4/m$ space group with $Z = 2$, $a = 13.350$ (1) Å, and $c = 9.738$ (2) Å. The structure was refined to $R_w = 0.043$. The complex features a trans configuration of the two fluorine atoms with D_{4h} symmetry and strict planarity of the porphyrin core. Typical bond lengths are Ti-N = 2.040 (4) Å and Ti-F = 1.788 (4) Å. XAFS spectra were recorded at the titanium K-edge for the series [(TPP)Ti^{IV}O], [(TPP)$Ti^{IV}X_2$], [(TPP)$Ti^{IV}(-O-)_2$Ph], [(TPP)$Ti^{IV}(-S-)_2$Tol], [(TPP)$Ti^{III}F_2]^-$, and [(TPP)Ti^{III}F].[1] Conventional data analyses failed to give satisfactory structural data due to destructive interferences resulting in ill-posed numerical problems. However, it was possible to extract reliable structural information by resorting to *perturbed difference* analyses, which take into account first-order distortions such as an axial shift of the metal. Interatomic distances between titanium and the axial ligands could be extracted with an absolute uncertainty of 0.02 Å and were in excellent agreement with the available crystal structure data.

1. Introduction[1]

Interest in the chemistry of titanium porphyrins stems essentially from the ability of these complexes to bind small molecules such as dioxygen.[2-4] Most insertions of titanium into a porphyrin free base unvaryingly yield very stable oxotitanium(IV) compounds[5] that cannot be used as starting materials for the synthesis of lower valent titanium porphyrins.[6] However, substitution of the axial oxo ligand can be achieved by reaction of hydrogen peroxide or hydrogen halides, leading to peroxo- or dihalogenotitanium(IV) porphyrin complexes, respectively.[7,8] The latter derivatives are better synthons for substitution reactions; moreover, they can be reduced chemically or electrochemically to titanium(III) species.[9]

The present investigation initially was concerned with the preparation and the physical and structural characterization of a series of dihalogenotitanium(IV) porphyrins. An earlier study at the Grenoble laboratories focused on their mass spectroscopic characterization with use of soft ionization methods.[10] It was shown that desorption-chemical ionization in the electron capture mode was particularly useful, since it avoided cleavage of axial bonds and afforded abundant molecular ions.[11] Early evidence concerning the structure of these compounds was obtained from ^{1}H NMR spectroscopy, which suggested a trans configuration of the halogeno ligands:[8] this configuration was confirmed by the X-ray crystal structure analysis[12] of [(TPP)$Ti^{IV}Br_2$]. At this point, we decided to investigate the possibility of obtaining some structural information on these compounds from extended X-ray absorption fine structure (EXAFS) spectroscopy.

Rapidly it turned out that conventional EXAFS analyses failed to give reliable results because the problem was numerically ill-conditioned or ill-posed if we refer to the stability criteria pointed out a long time ago by Hadamard and extensively developed by Tikhonov and Arsenin.[13] In a simple language, information can be lost through destructive interferences, whereas the EXAFS modulation cannot be measured over a large enough k range to allow individual contributions of overlapping shells to be well resolved. A possible way to resolve this ambiguous situation is to combine the information contained in several spectra by resorting to refined comparative or difference methods that take advantage of the well-proved sensitivity of EXAFS to small structural details. Whereas the information content obviously increases with the number of spectra to be compared, only a reduced number of parameters is often sufficient for describing the structural changes that can be detected in EXAFS spectra. Successful illustrations of this strategy have been reported by Goulon et al.[14-18] In metalloporphyrins, one is usually most

[†] Laboratoire de Chimie de Coordination, Centre d'Etudes Nucléaires de Grenoble.
[‡] Service de Physique/Structure, Centre d'Etudes Nucléaires de Grenoble.
[§] Université de Nancy-I.
[∥] LURE, Université de Paris-Sud/Orsay.
[⊥] Present address: ESRF, B. P. 220, F-38043 Grenoble Cedex, France.

(1) Abbreviations used in this paper: TPP = tetraphenylporphyrinato; OEP = octaethylporphyrinato; $(-O-)_2$Ph = catecholato; $(-S-)_2$Tol = 3,4-toluenedithiolato; Por = porphyrinato; EXAFS = X-ray absorption fine structure; XANES = X-ray absorption near-edge structure; SS = single scattering; MS = multiple scattering; INDO/S, intermediate neglect of differential overlap for (electron) spectroscopy.

(2) Guilard, R.; Lecomte, C. *Coord. Chem. Rev.* **1985**, *65*, 87-113.
(3) Gubelmann, M. H.; Williams, A. F. *Struct. Bonding* **1983**, *55*, 1-65.
(4) Holm, R. H. *Chem. Rev.* **1987**, *87*, 1401-1449.
(5) Fournari, P.; Guilard, R.; Fontesse, M.; Latour, J. M.; Marchon, J. C. *J. Organomet. Chem.* **1976**, *110*, 205-217.
(6) Malinski, T.; Chang, D.; Latour, J. M.; Marchon, J. C.; Gross, M.; Giraudeau, A.; Kadish, K. M. *Inorg. Chem.* **1984**, *23*, 3947-3955.
(7) Guilard, R.; Latour, J. M.; Lecomte, C.; Marchon, J. C.; Protas, J.; Ripoll, D. *Inorg. Chem.* **1978**, *17*, 1225-1235.
(8) Nakajima, M.; Latour, J. M.; Marchon, J. C. *J. Chem. Soc., Chem. Commun.* **1977**, 763-764.
(9) Latour, J. M.; Marchon, J. C.; Nakajima, M. *J. Am. Chem. Soc.* **1979**, *101*, 3974-3976.
(10) Forest, E.; Ulrich, J.; Marchon, J. C.; Virelizier, H. *Org. Mass Spectrom.* **1987**, *22*, 45-48.
(11) Forest, E.; Marchon, J. C.; Ulrich, J.; Virelizier, H. *Inorg. Chem.* **1986**, *25*, 3570-3572.
(12) Lecomte, C.; Protas, J.; Marchon, J. C.; Nakajima, M. *Acta Crystallogr., Sect. B: Struct. Crystallogr. Cryst. Chem.* **1978**, *34*, 2856-2858.
(13) Tikhonov, A. N.; Arsenin, V. H. *Solution of Ill-Posed Problems*; Wiley: New York, 1977.
(14) Goulon, J.; Loos, M.; Friant, P.; Ruiz-Lopez, M. F. In *Chemical Crystallography with Pulsed Neutrons and Synchrotron X-rays*; Carrondo, M. A., Geffrey, G. A., Eds.; NATO ASI Series C; D. Reidel: Dordrecht, The Netherlands, 1988; No. 221, pp 247-293.
(15) Goulon, J.; Loos, M.; Ascone, I.; Goulon-Ginet, C.; Battioni, P.; Battioni, J. P.; Mahy, J. P.; Mansuy, D.; Meunier, B. In *Biophysics and Synchrotron Radiation*; Bianconi, A., Congiu-Castellano, A., Eds.; Springer Series in Biophysics 2; Springer-Verlag: West Berlin, 1987; pp 191-200.
(16) Goulon, J.; Friant, P.; Goulon-Ginet, C.; Coutsolelos, A.; Guilard, R. *Chem. Phys.* **1984**, *83*, 367-375.

0020-1669/90/1329-0057$02.50/0

interested in the coordination of the metal by the axial ligands and it is indeed attractive to let the signatures of the macrocyclic ring cancel out in a difference. Unfortunately, in the case of asymmetrical axial ligation, the metal is often slightly shifted out of the average porphyrin plane and direct differences become totally unsuccessful. It is nevertheless a rather trivial exercise to "perturb" the experimental spectrum so as to shift artificially the metal back to the porphyrin plane until the intense signatures of the porphyrin ring can cancel out properly in a difference.[16] On the other hand, it is now well documented that a porphyrin ring is not strictly rigid: (i) a very small adjustment of the macrocyclic cavity radius (≤0.02 Å) can result from a so-called "ruffling" of the pyrrole units, whereas (ii) second-order "doming" distortions have also been reported. We certainly do not claim that difference analyses of EXAFS spectra can yield an accurate description of such second-order distortions: with reference to the extensive literature on the structure of metalloporphyrins, our goal is merely to check whether a crude modelization of these small *perturbations* can produce "cleaner" difference spectra with an improved cancellation of all intense signatures of the porphyrin pattern. As a consequence, we expect the assignment and analyses of the weak contributions of the axial ligands to become easier and more accurate.

For the sake of corroboration, the structure of $[(TPP)Ti^{IV}F_2]$ was determined from X-ray crystallography, which made it possible to assess the reliability of EXAFS difference analyses. As the comparison with indisputable crystallographic data proved to be successful, we felt encouraged to carry on with the same strategy for characterizing the structure of several titanium(IV) or titanium(III) porphyrin complexes by EXAFS spectroscopy.

2. Experimental Section

2.1. Materials. Conversion of the titanyl porphyrin complexes to the corresponding dihalogenotitanium(IV) complexes was obtained by a general procedure, which is described below for the difluoro complex of (tetraphenylporphyrinato)titanium(IV).

Difluoro(tetraphenylporphyrinato)titanium(IV). Dinitrogen was bubbled through a 50% HF aqueous solution (200 mL), and the outgoing gaseous N_2/HF mixture was passed for 30 min successively through 500 mL of hexane and through a solution of 500 mg of [(TPP)TiO] in dichloromethane. The porphyrin solution turned from pink to dark green. Dropwise addition of the HF-saturated hexane to the porphyrin solution yielded a green microcrystalline powder, which was filtered and dried under dry dinitrogen; yield 406 mg (79%). Anal. Found (calcd) for $C_{44}H_{28}N_4TiF_2$: C, 75.55 (75.65); H, 4.17 (4.04); N, 7.98 (8.02); Ti, 6.68 (6.86); F, 4.90 (5.44). IR ν_{Ti-F} = 647 cm^{-1}. The dichloro complexes were prepared by a similar procedure. Gaseous HBr for the synthesis of the dibromo derivative was produced by the reaction of Br_2 with 1,2,3,4-tetrahydronaphthalene.

(Catecholato)- and (3,4-Toluenedithiolato)(tetraphenylporphyrinato)titanium(IV). These complexes were prepared from the oxotitanium(IV) tetraphenylporphyrin and either catechol or 3,4-toluenedithiol according to the procedure described by Deronzier and Latour.[19]

Fluoro(tetraphenylporphyrinato)titanium(III). This compound was prepared by a zinc amalgam reduction of $[(TPP)TiF_2]$ with use of a procedure detailed elsewhere by Marchon et al.[20]

Tetrabutylammonium Difluoro(tetraphenylporphyrinato)titanate(III). This complex was prepared in a glovebox under argon by addition in small aliquots of a stoichiometric amount of $Bu_4NF{\cdot}3H_2O$ to a benzene solution of **7**. The difluoro complex precipitated immediately; fluoride addition was continued until the solution turned colorless. The turquoise blue precipitate was filtered and dried. Anal. Found (calcd) for $(Bu_4N)[(TPP)TiF_2]{\cdot}H_2O$: C, 75.14 (74.95); H, 6.94 (6.67); N, 7.30 (7.51); Ti, 4.99 (4.64).

Hereafter the following identification code will be used: **1**, $[(TPP)Ti^{IV}{=}O]$; **2**, $[(TPP)Ti^{IV}F_2]$; **3**, $[(TPP)Ti^{IV}Cl_2]$; **4**, $[(TPP)Ti^{IV}Br_2]$; **5**, $[(TPP)Ti^{IV}(-O-)_2Ph]$; **6**, $[(TPP)Ti^{IV}(-S-)_2Tol]$; **7**, $[(TPP)Ti^{III}F]$; **8**, $[(TPP)Ti^{III}F_2]^-Bu_4N^+$.

Table I. Crystallographic Data for $(TPP)TiF_2$

chem formula: $C_{44}H_{28}N_4F_2Ti$	radiation: Mo Kα (λ = 0.71069 Å)
fw: 698.637	Ge monochromator
space group: $I4/m$	ρ_{calcd} = 1.337 g cm^{-3}
a = 13.350 (1) Å	ρ_{obsd}: not measd
c = 9.738 (2) Å	μ: not measd
V = 1735.53 $Å^3$	$R(F_o)$ = 8.0%
Z = 2	$R_w(F_o)$ = 4.3%
T = 293 K	

2.2. Spectroscopic and Electrochemical Characterization. Infrared spectra were recorded as 0.5% dispersions in KBr or CsI with a Beckman IR 4240 spectrometer. UV–visible spectra were run on a Beckman Acta IV spectrophotometer. ^1H NMR spectra were recorded at 250 MHz on a Cameca 250 spectrometer operating in the Fourier transform mode and requiring the accumulation of 200 transients.

Electrochemical measurements were made in a three-electrode configuration with Tacussel instrumentation. The dichloromethane solvent was carefully dried over neutral alumina. The tetrabutylammonium hexafluorophosphate ($Bu_4N^+PF_6^-$) supporting electrolyte was recrystallized from dry dichloromethane before use.

2.3. Crystal Structure Determination. A preliminary Weissenberg photographic assay on a suitable crystal of $[(TPP)Ti^{IV}F_2]$ (**2**) indicated tetragonal symmetry. Unit cell dimensions were obtained by least-squares refinement of the 2θ values for 25 reflections having $2\theta > 20°$. The crystal characteristics and the data collection and refinement details are summarized in Table I. Intensities were corrected for Lorentz and polarization effects, but no absorption correction was applied.

The structure was solved by assuming that it was isotypic with that of $[(TPP)Ti^{IV}Br_2]$ (**4**).[12] The atomic coordinates of the latter complex (except for the F atom, which was placed at a suitable distance from the Ti atom) were introduced, as input guess coordinates, for the initial refinement cycle. Isotropic refinement of all non-hydrogen atoms was the first step. Anisotropic thermal parameters were then included for all non-hydrogen atoms. In the final cycles of refinement, the positions of the hydrogen atoms were preset at their calculated positions with fixed isotropic thermal parameters of 5 $Å^2$. The final agreement factors are given in Table I.

2.4. X-ray Absorption Spectroscopy. 2.4.1. Data Collection. X-ray absorption spectra were recorded in 1984 at LURE (i.e. the French National Synchrotron Radiation Facility) on the "EXAFS-II" spectrometer. The key component of this spectrometer is a two-separated-crystal monochromator that was equipped (for the present experiments) with a pair of Si-111 single crystals limiting the energy resolution to modest performances, $1._1$ eV (XANES) ≤ $\Delta E \leq 2._3$ eV (EXAFS), even though the distance between the entrance and exit slits was kept very long (3 m).[21] An efficient harmonic rejector consisting of two plane parallel mirrors with variable grazing incidence angles was systematically used.[22] All the spectra discussed in this paper were recorded in the conventional absorption mode with He–Ne-filled ion chambers operating in a strictly linear regime. The energy calibration made reference to the XANES spectrum of a titanium metal foil, which exhibits a well-resolved pre-edge shoulder peaking at an energy arbitrarily set to 4965.5 eV.

Ca. 25 mg of each sample was pressed in special forms in order to obtain pellets of the appropriate geometry (17 × 5 mm^2), which were carefully checked for homogeneity and for the absence of microfractures. These pellets were then sandwiched between two extrathin (3 μm) polycarbonate windows and held in a cardboard slide holder. For air-sensitive titanium(III) samples, the slide holder was inserted in a sealed polyethylene bag kept under argon.

2.4.2. Data Analyses. The experimental EXAFS spectra were analyzed at the University of Nancy-I following standard procedures detailed elsewhere.[14] In our experience, the quality and readability of the FT spectra Im[$\tilde{\chi}(R)$] (where Im = imaginary part) is often significantly improved when these spectra are corrected according to eq 1 for the phase-shift and back-scattering amplitude functions relevant for the dominant shell j.

$$\tilde{\chi}_{(n)j}(R) = \int_0^\infty w(\mathbf{k})\, \chi(\mathbf{k}) \frac{\mathbf{k}\bar{R}_j^2}{\bar{N}_j F_j(\mathbf{k})\, A_j} \exp[2\sigma_j^2\mathbf{k}^2 - 2i\mathbf{k}R - i\,\psi_j(\mathbf{k})]\, \mathbf{dk} \quad (1)$$

(17) Friant, P.; Goulon, J.; Fischer, J.; Ricard, L.; Schappacher, M.; Weiss, R.; Momenteau, M. *Nouv. J. Chim.* **1985**, *9*, 33–40.
(18) Bortolini, O.; Ricci, M.; Meunier, B.; Friant, P.; Ascone, I.; Goulon, J. *Nouv. J. Chim.* **1986**, *10*, 39–49.
(19) Deronzier, A.; Latour, J. M. *Nouv. J. Chim.* **1984**, *8*, 393–399.
(20) Marchon, J. C.; Latour, J. M.; Boreham, C. J. *J. Mol. Catal.* **1980**, *7*, 227–233.
(21) Goulon, J.; Lemonnier, M.; Cortes, R.; Retournard, A.; Raoux, D. *Nucl. Instrum. Methods* **1983**, *208*, 625–630.
(22) Goulon, J.; Cortes, R.; Retournard, A.; George, A.; Battioni, J. P.; Frety, R.; Moraweck, B. In *EXAFS and Near Edge Structure III*; Hodgson, K., Hedman, B., Penner-Hahn, J. E., Eds.; Springer Proceedings in Physics 2; Springer-Verlag: West Berlin, 1984; pp 449–451.

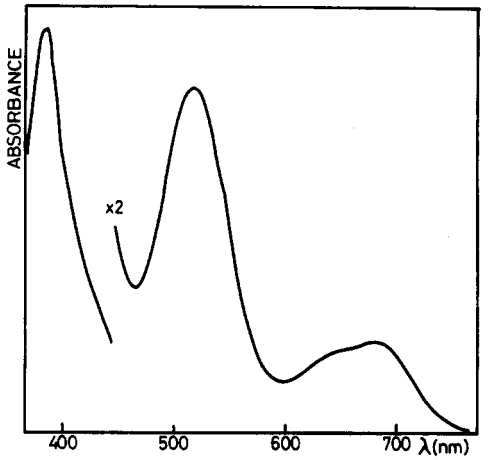

Figure 1. Visible absorption spectrum of $[(TPP)Ti^{IV}F_2]$ in dichloromethane.

In eq 1 $w(\mathbf{k})$ denotes a Kaiser–Bessel window function minimizing the well-known side-lobe effects due to the finite data range in momentum space, whereas $F_j(\mathbf{k})$ and $\psi_j(\mathbf{k})$ are standard notation for the scattering amplitude and total phase-shift functions, which were calculated for shell j from the crude parameterization proposed by Teo et al.[23] In the case of metalloporphyrins, the FT spectra are most often dominated by the single scattering (SS, $n = 2$) contribution of the four equatorial nitrogen atoms of the macrocyclic ligand. For the sake of clarity, *all* the FT spectra reproduced in this paper are systematically corrected for this particular shell; i.e. for $j = 1$, $\bar{N}_j = 4$. The energy offset E_0 involved in the definition of the photoelectron wave vector $\mathbf{k} = [2m\hbar^2(E_{RX} - E_0)]^{1/2}$ should normally be adjusted self-consistently according to the so-called Lee and Beni criterion of coincidence between the maxima of Im $[\tilde{\chi}_{(2):1}(R)]$ and $|\tilde{\chi}_{(2):1}(R)|$.[24] In our case, however, this recipe is useless because the signal of the axial ligands strongly interferes with that of the equatorial nitrogen atoms. Our strategy was therefore to select E_0 so that the characteristic signatures of the light atoms of the porphyrin macrocycle (i.e. the signatures of 4 N, 8 C_A, 4 C_{meso}, and 8 C_B) exhibit similar phases in the corrected FT spectrum of complex **1**. The same value of E_0 was then kept for all subsequent FT analyses of all titanium(IV) complexes **2–6**. In eq 1 $\bar{R}_j$ and $\sigma_j^2 = \langle(R_j - \bar{R}_j)^2\rangle$ are guesses for the first and second moments of the distance distribution due to thermal disorder: in practice, $\bar{R}_j$ and σ_j^2 were preset to some reasonable values and then kept fixed (again for the sake of comparison). On the other hand, $A_j(\mathbf{k})$ refers to a semiempirical factor accounting crudely for inelastic losses and electronic relaxation effects.[14,25] Corrections yielding FT spectra consistent with the curved-wave formalism were not considered here.[26]

More details are given elsewhere[14,15] on the difference analyses and on the models used for the ruffling and doming distortions of porphyrins. As shown in the Appendix, errors could be estimated in our difference analyses with the same level of validity as in standard fits. Note that the basic formulation given in the Appendix does not include yet additional constraints resulting from any "prior knowledge" about the chemistry of our system, e.g. about the nature of the axial ligands which implies strong constraints regarding the phase of the difference spectrum. This extension will be considered elsewhere.[27]

Nonlinear least-squares fitting routines (delivering systematically the residual factor of the fit and the full correlation matrix between the adjusted parameters) are optionally available and can be used for refining the analyses of the difference spectra in the momentum space.[14] Of course, at this stage of refinement, E_0 may need to be slightly readjusted in order to account for the specific nature of a given scatterer.

3. Results and Discussion

3.1. Spectroscopic Characterization and Electrochemical Data. 3.1.1. Dihalogenotitanium(IV) Porphyrin Complexes. The reaction of hydrogen halides with titanyl porphyrins in dry dichloromethane leads to pure, crystalline dihalogenotitanium(IV) porphyrin complexes. The latter are, however, easily hydrolyzed in solution back to the parent oxo complex, but less so in the crystalline state. Stability toward hydrolysis decreases according to the sequence F > Cl > Br.[11] Infrared spectroscopy is convenient for checking the purity of the final substitution product: the characteristic Ti=O stretching vibration of the titanyl complex (e.g. $\nu_{Ti=O}$(Por = TPP) = 981 cm^{-1}, $\nu_{Ti=O}$(Por = OEP) = 966 cm^{-1} was absent in the IR spectra of the dihalogeno complexes, whereas new absorption bands due to the titanium–halogen stretching vibrations were detected in the far-infrared region. The corresponding frequencies are listed in Table II for the two series of ligands Por = TPP and Por = OEP. As reflected by the systematically higher frequencies quoted in Table II, the TPP complexes are less flexible than the OEP derivatives.

Table II. Infrared Stretching Frequencies (cm^{-1}) of Titanium–Halogen Bonds in Dihalogenotitanium(IV) Porphyrins $(P)TiX_2$ (P = TPP, OEP; X = F, Cl, Br)

	$(TPP)TiX_2$	$(OEP)TiX_2$
ν_{Ti-F}	647	639
ν_{Ti-Cl}	358	330
ν_{Ti-Br}	280	240

Table III. Absorption Maxima (nm) in the Visible Range (300–800 nm) and Corresponding Absorption Coefficients (10^{-4} mol^{-1} L cm^{-1}) of $(TPP)TiX_2$ (X = F, Cl, Br) in Dichloromethane with an Excess of HX

$(TPP)TiF_2$	λ_{max}	340	387	498	650	690 (sh)
	ϵ	5.5	7.0	3.0	0.9	
$(TPP)TiCl_2$	λ_{max}	322	375	496	520 (sh)	692
	ϵ	3.4	14.1	1.9		0.5
$(TPP)TiBr_2$	λ_{max}	328	381	506	531 (sh)	730
	ϵ	3.3	13.7	1.6		0.4

Table IV. ^1H NMR Shifts (δ, ppm vs TMS) for the $(TPP)TiX_2$ Complexes

	pyrr	Ph *o*-H	Ph *m*, *p*-H
$(TPP)TiF_2$	9.00 (s)	8.30 (s)	7.82–7.80 (m)
$(TPP)TiCl_2$	9.07 (s)	8.29 (s)	7.86–7.83 (m)
$(TPP)TiBr_2$	9.12 (s)	8.30 (s)	7.86–7.83 (m)

Table V. Half-Wave Potentials of Difluorotitanium(IV) Porphyrin Complexes in Dichloromethane Solution (V vs SCE)

	$P^{2-} \leftarrow P^{\bullet-}$	$P^{\bullet-} \leftarrow P$	$Ti^{III} \leftarrow Ti^{IV}$	$P \rightarrow P^{\bullet+}$	$P^{\bullet+} \rightarrow P^{2+}$
$(TPP)TiF_2$	−1.98	−1.53	−0.45	+1.25	+1.82
$(OEP)TiF_2$		−1.75	−0.56	+1.16	+1.76

The visible spectrum of $[(TPP)Ti^{IV}F_2]$ (**2**) is shown in Figure 1, and the wavelengths and extinction coefficients at the absorption maxima are listed in Table III for the whole series **2–4**. As evidenced by the split Soret band in the 300–400-nm range, none of these complexes show a normal porphyrin spectrum in Gouterman's terminology.[28]

^1H NMR spectra confirm the expected diamagnetism of these d^0 Ti(IV) complexes. The chemical shifts of the major lines are listed in Table IV for the whole series. The fact that one observes a *single* resonance for the ortho phenyl protons is of particular interest: this is indeed consistent with the D_{4h} symmetry of all $[(TPP)Ti^{IV}X_2]$ complexes, i.e. with a trans configuration of the halogen atoms.[8,12]

In dry dichloromethane solution, the difluorotitanium(IV) complexes exhibit three one-electron-reduction waves and two one-electron-oxidation waves at a rotating-platinum-disk electrode. Each of these redox steps is reversible on the time scale of cyclic voltammetry. The values of the corresponding half-wave potentials are listed in Table V for $[(TPP)Ti^{IV}F_2]$ and $[(OEP)Ti^{IV}F_2]$. Controlled-potential electrolysis at a potential located on the plateau located on the plateau of the first reduction wave, e.g. −0.9 V for $[(TPP)Ti^{IV}F_2]$ or −1.0 V for $[(OEP)Ti^{IV}F_2]$, requires 1.0 faraday/mol of the complex. Visible spectra recorded at intermediate stages of reduction of $[(TPP)Ti^{IV}F_2]$ exhibit isosbestic

(23) Teo, B. K.; Lee, P. A.; Simmons, A. L.; Eisenberger, P.; Kincaid, B. *J. Am. Chem. Soc.* **1977**, *99*, 3854–3859.
(24) Lee, P. A.; Beni, G. *Phys. Rev.* **1977**, *B15*, 2862–2883.
(25) Stern, E. A.; Heald, S. M.; Bunker, B. *Phys. Rev. Lett.* **1979**, *42*, 1372–1375.
(26) Loos, M.; Brouder, C.; Goulon, J. *Physica B+C* **1989**, *B158*, 276–278.
(27) Goulon, J. Unpublished work.
(28) Gouterman, M. In *The Porphyrins*; Dolphin D., Ed.; Academic Press: New York, 1978; Vol. III, pp 1–165.

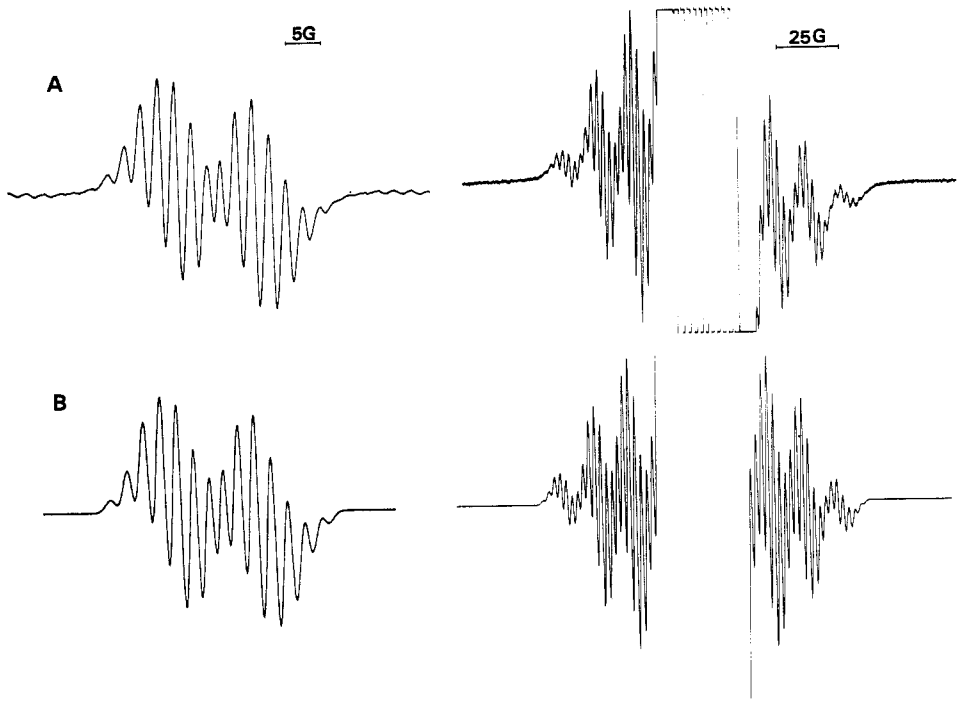

Figure 2. ESR spectra of [(TPP)Ti^{III}F]: (A) experimental spectra in toluene at room temperature (left, central part of spectrum; right, detailed side bands); (B) simulated spectra (left, central part; right, detailed side bands). Values of a_F, a_N, and a_{Ti} used for simulation are listed in Table VI.

Table VI. EPR Parameters of Titanium(III) Porphyrin Complexes[a]

complex	g	a_F, G	a_N, G	a_L, G (nucleus)
(TPP)TiF	1.972	11.19	2.28	13.93 (^{47,49}Ti)
[(TPP)TiF$_2$]$^-$	1.968	6.7	2.20	6.7 (F)
(OEP)TiF	1.973	10.9	2.34	
[(OEP)TiF$_2$]$^-$	1.971	6.3	2.25	6.3 (F)
(TPP)TiF(THF)	1.965	9.6	2.35	
(TPP)TiF(py)	1.964	9.5	2.2	1.0 (N)
(TPP)TiF(1-MeIm)	1.961	9.8	2.5	1.0 (N), 0.7 (N)
(TPP)TiF(NMP)	1.963	9.8	2.4	0.7 (N)
(TPP)TiF(PBu$_3$)	1.970	9.0	2.35	0.84 (P)

[a] Abbreviations: THF, tetrahydrofuran; py, pyridine; 1-MeIm, 1-methylimidazole; NMP, *N*-methylpyrrolidinone; PBu$_3$, tributylphosphine.

points at 458, 574, 606, 618, and 643 nm. The reduced solution exhibits an oxidation wave at a potential identical with that of the first reduction wave of the starting complex. Such a behavior is consistent with an electron transfer devoid of coupled chemical reactions and therefore suggests that the parent and reduced complexes should have similar structures. The reduced complex is then presumably an anionic difluorotitanium porphyrin complex. Insofar as the second and third reduction waves are associated with reduction steps of the macrocyclic ring, we conclude that the product of the first electrochemical reduction is a titanium(III) complex. This interpretation is confirmed by the examination of its ESR spectrum (vide infra). On the other hand, it is noteworthy that the value of the potential range between the first ring reduction and the first ring oxidation, $\Delta E_{1/2}$ = 2.8–2.9 V, is much larger than the "normal"[29] value ($\Delta E_{1/2}$ = 2.2$_3$ V) and is consistent with the anomalous electronic spectra of these complexes.

3.1.2. Titanium(III) Porphyrin Complexes. ESR spectra gave us reliable evidence that in **2** the titanium atom is the actual site of electron transfer on chemical[9,20] or electrochemical[9] reduction. Both the experimental and simulated ESR spectra are shown in Figure 2 for the pentacoordinated complex **7** and in Figure 3 for the difluoro species **8**. The corresponding ESR spectral parameters are summarized in Table VI. Note that the values found for the coupling constants a_{Ti}, a_N, and a_F are indeed consistent with the assignment of both **7** and **8** as titanium(III) complexes.

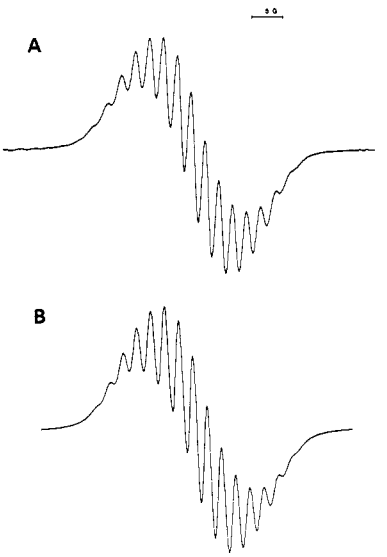

Figure 3. ESR spectra of [(TPP)Ti^{III}F$_2$]$^-$Bu$_4$N$^+$: (A) experimental spectrum in dichloromethane at room temperature; (B) simulated spectrum.

The lowest occupied state in which the unpaired electron resides in titanium(III) porphyrin complexes is usually described as a molecular orbital involving the metal 3d$_{xy}$ atomic orbital. Several ESR studies have also been reported on the isoelectronic oxovanadium(IV) porphyrin[30-34] or on 4d^1 molybdenum(V) porphyrin complexes:[35-37] they have all been interpreted again in terms of a singly occupied "d$_{xy}$"-like state, and this assignment has been

(29) Fuhrhop, J. H.; Kadish, K. M.; Davis, D. G. *J. Am. Chem. Soc.* **1973**, *95*, 5140–5147.
(30) Kivelson, D.; Lee, S. K. *J. Chem. Phys.* **1964**, *41*, 1896–1903.
(31) Assour, J. M. *J. Chem. Phys.* **1965**, *43*, 2477–2489.
(32) Assour, J. M.; Goldmacher, J.; Harrison, S. E. *J. Chem. Phys.* **1965**, *43*, 159–165.
(33) Lau, P. W.; Lin, W. C. *J. Inorg. Nucl. Chem.* **1975**, *37*, 2389–2398.
(34) Poncet, J. L.; Guilard, R.; Friant, P.; Goulon-Ginet, C.; Goulon, J. *Nouv. J. Chim.* **1984**, *8*, 583–590.
(35) Newton, C. M.; Davis, D. G. *J. Magn. Reson.* **1975**, *20*, 446–457.
(36) Matsuda, Y.; Kubota, F.; Murakami, Y. *Chem. Lett.* **1977**, 1281–1284.
(37) Hayes, R. G.; Scheidt, W. R. *Inorg. Chem.* **1978**, *17*, 1082–1084.

Table VII. Atomic Coordinates in the Unit Cell of $(TPP)TiF_2$

atom	10^4x	10^4y	10^4z	B_{eq}, Å^2
Ti	0 (0)	0 (0)	0 (0)	3.64
F	0 (0)	0 (0)	−1836 (4)	5.45
N(1)	1484 (3)	−360 (3)	0 (0)	3.55
C(1)	1887 (4)	−1321 (4)	0 (0)	3.77
C(2)	2969 (4)	−1254 (4)	0 (0)	4.19
C(3)	3206 (4)	−269 (4)	0 (0)	4.27
C(4)	2283 (4)	295 (4)	0 (0)	3.77
C(5)	2210 (4)	1340 (4)	0 (0)	3.95
C(6)	3179 (4)	1924 (4)	0 (0)	3.69
C(7)	3614 (3)	2199 (3)	1218 (4)	5.66
C(8)	4494 (3)	2761 (3)	1203 (5)	6.70
C(9)	4911 (4)	3034 (5)	0 (0)	5.81
HC(2)	3560	−1890	0	
HC(3)	3950	60	0	
HC(7)	1790	−3180	−2110	
HC(8)	2850	−4890	−2190	
HC(9)	3460	−5630	0	

supported by extended Hückel or INDO/S calculations.[38,39] Unrestricted Hartree–Fock INDO/S calculations[39,40] were performed at the University of Nancy (see section 3.3.3) for both the (closed-shell) titanium(IV) complex **1** and for the low-valent (open-shell) titanium(III) complex **7**: these calculations were carried out on the basis of the structural data derived from our EXAFS investigations, and they confirmed unambiguously that for these two systems, having the C_{4v} point group symmetry, the lowest unoccupied 3d-like orbital in complex **1** and the highest occupied orbital in complex **7** were molecular orbitals of B_2 symmetry strongly dominated by the $3d_{xy}$ atomic orbital of the metal ($C_{d_{xy}}^2 \geq 95\%$). However, we wish to stress the fact that this description does not necessarily hold for *all* vanadium(IV) or titanium(III) compounds: quite to the contrary, concerning the complex $[(Por)V^{IV}Cl_2]$, INDO-S calculations[40] suggest that the lowest occupied orbital is a doubly degenerate state of symmetry E_g built with atomic orbitals of V ($3d_{xz}$, $3d_{yz}$), Cl ($3p_x$, $3p_y$), and C ($2p_z$) in this case: indeed, one may expect spin–orbit coupling or Jahn–Teller effects to remove such an orbital degeneracy and to produce excited states lying only a few wavenumbers above the ground state. This probably explains why no ESR spectrum has yet been detected for the isoelectronic series $[(Por)V^{IV}X_2]$, even at liquid-nitrogen temperature:[40] nearby excited states lead to very short T_1 values and, hence, very broad absorption lines.

Concerning the ESR spectra of species **7** and **8**, we observe that the small value of the hyperfine coupling constants due to the four equivalent nitrogen nuclei of the porphyrin macrocycle, a_N = 2.2–2.5 G, is fairly consistent with the assignment of the ground state to a d_{xy}-like orbital. On the other hand, the hyperfine coupling constant with the axial fluorine ligand in $[(TPP)Ti^{III}F]$ (**7**) is substantially larger: this result indicates a low electron spin density at the fluorine nucleus, whose magnetic moment is large,[41] and again supports the proposed electronic configuration. One may note that the fluorine hyperfine coupling constants observed for the anionic species $[(Por)Ti^{III}F_2]^-Bu_4N^+$ (i.e. a_F = 6.3–6.7 G) are comparable with the value a_F = 7.5 G) reported for $[(H_2O)_4Ti^{III}F_2]^+$.[42]

The five-coordinate titanium(III) complex **7** is a versatile starting material for the synthesis of a number of axially ligated titanium(III) porphyrins. Addition of ligands such as fluoride, tetrahydrofuran, nitrogen bases, and phosphines has been reported earlier;[9] axial substitution of the fluorine atom was achieved with benzenethiolate,[20] phenyl, *o*-tolyl, and benzyl,[43] methoxide,[44] and catecholate and *o*-toluenedithiolate.[19] Finally, one should also mention that interconversion between titanium(III) porphyrins and titanium(IV) porphyrin anion radicals has been observed: this possibility was related to the nonchelating versus chelating coordination ability of the axial ligand.[19]

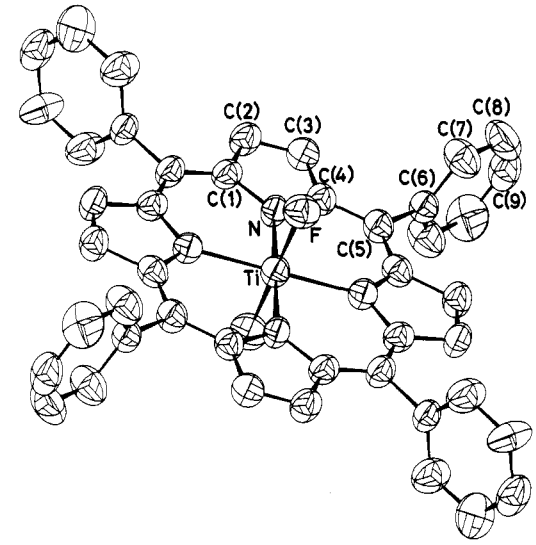

Figure 4. ORTEP view of a $[(TPP)Ti^{IV}F_2]$ molecule. The vibrational ellipsoids are drawn at the 50% probability level.

Table VIII. Selected Bond Lengths (Å) and Bond Angles (deg) for $(TPP)TiF_2$

Ti–F	1.788 (4)	Ti–N	2.040 (4)
N–C(1)	1.391 (6)	N–C(4)	1.379 (6)
C(1)–C(2)	1.447 (7)	C(3)–C(4)	1.445 (7)
C(2)–C(3)	1.353 (7)	C(4)–C(5)	1.399 (7)
C(1)–C(5′)	1.394 (7)	C(5)–C(6)	1.511 (7)
C(6)–C(7)	1.371 (5)	C(7)–C(8)	1.395 (5)
C(8)–C(9)	1.347 (5)		
C(1)–N–C(4)	106.64 (4)	N–C(1)–C(2)	109.2 (5)
N–C(1)–C(5′)	125.6 (5)	C(2)–C(1)–C(5′)	125.1 (6)
C(1)–C(2)–C(3)	107.0 (5)	C(2)–C(3)–C(4)	107.9 (5)
N–C(4)–C(5)	125.4 (6)	N–C(4)–C(3)	109.2 (4)
C(3)–C(4)–C(5)	125.4 (6)	C(4)–C(5)–C(6)	117.1 (5)
C(4)–C(5)–C(1′)	125.6 (5)	C(1)–C(5)–C(6)	117.3 (5)
C(5)–C(6)–C(7)	120.0 (3)	C(6)–C(7)–C(8)	119.4 (5)
C(7)–C(8)–C(9)	120.2 (5)	C(8)–C(9)–C(8′)	120.8 (6)
C(7)–C(6)–C(7′)	119.9 (6)		

3.2. Crystal Structure of 2. The crystal structure of $[(TPP)Ti^{IV}F_2]$ (**2**) indicates the presence of discrete molecules in which the titanium atom exhibits the expected octahedral coordination (4 N + 2 F). Since this compound crystallizes in the tetragonal space group $I4/m$ with the titanium atom at the inversion center, the coordination polyhedron has to be consistent with D_{4h} symmetry; i.e., a strict porphyrin planarity and the trans configuration of the two fluorine atoms are implicit. This structure is isotypic with that of **4**, which was determined by Lecomte et al.[12] A plot of the molecule **2**, with the labeling code, is shown in Figure 4. Fractional coordinates are listed in Table VII, and selected structural parameters are summarized in Table VIII. From the values quoted in Table VIII, it appears that the average Ti–N distance might be shorter (by ca. −0.02 Å) than in the structure of the dibromo derivative **4**.[12] This small difference is not really significant if one takes into consideration the admitted limits of uncertainty (i.e. 3 times the standard deviations) for both structural determinations: $R_{Ti-N}(2) = 2.0_4 \pm 0.01_2$ Å, $R_{Ti-N}(4) = 2.0_6 \pm 0.02_4$ Å. In any case, the space group $I4/m$ itself prevents the crystallographic detection of any "ruffling" of the porphyrin core.

It is noteworthy that the dichloro complex of titanium(IV) phthalocyanine, $[(Pc)Ti^{IV}Cl_2]$, features a cis configuration of the

(38) Zerner, M.; Gouterman, M. *Inorg. Chem.* **1966**, *5*, 1699–1706.
(39) Ruiz-Lopez, M. F.; Rinaldi, D.; Esselin, C.; Goulon, J.; Poncet, J. L.; Guilard, R. *J. Phys. Colloq.* **1986**, *47*(C8), 637–640.
(40) Richard, P.; Poncet, J. L.; Barbe, J. M.; Guilard, R.; Goulon, J.; Rinaldi, D.; Cartier, A.; Tola, P. *J. Chem. Soc., Dalton Trans.* **1982**, 1451–1456.
(41) Morton, J. R.; Preston, K. F. *ACS Symp. Ser.* **1978**, *No. 66*, 386–409.
(42) Premovic, P. I.; West, P. R. *Can. J. Chem.* **1975**, *53*, 1593.
(43) Latour, J. M.; Boreham, C. J.; Marchon, J. C. *J. Organomet. Chem.* **1980**, *190*, C61–C63.
(44) Boreham, C. J.; Buisson, G.; Duée, E.; Jordanov, J.; Latour, J. M.; Marchon, J. C. *Inorg. Chim. Acta* **1983**, *70*, 77–82.

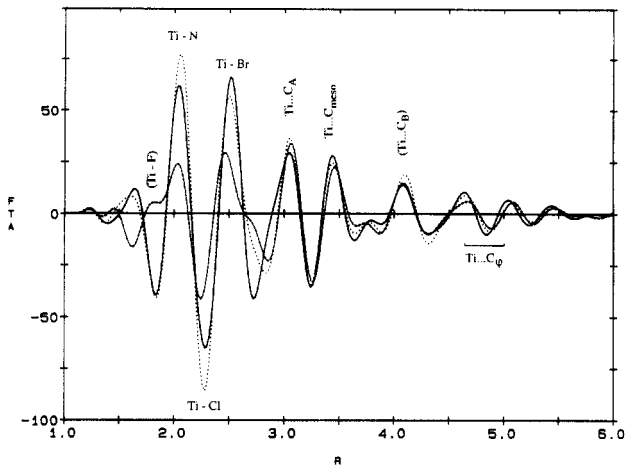

Figure 5. FT Im $[\tilde{\chi}_{(2):1}(R)]$ spectra for the whole series $[(TPP)Ti^{IV}(X)_2]$: (---) $[(TPP)Ti^{IV}F_2]$ (**2**); (···) $[(TPP)Ti^{IV}Cl_2]$ (**3**); (—) $[(TPP)Ti^{IV}Br_2]$ (**4**).

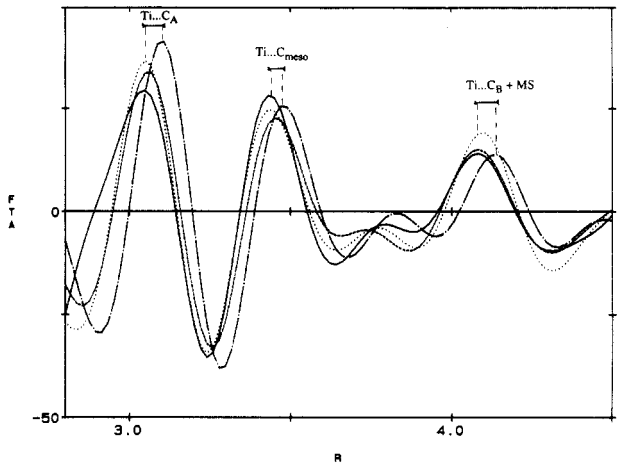

Figure 6. Expanded-scale comparison of the C_A, C_{meso}, and C_B signatures for (—) $[(TPP)Ti^{IV}Br_2]$ (**4**), (···) $[(TPP)Ti^{IV}Cl_2]$ (**3**), (---) $[(TPP)Ti^{IV}F_2]$ (**2**), and (·–·) $[(TPP)Ti^{IV}{=}O]$ (**1**). The titanium atom is clearly shifted out of the porphyrin mean plane in the reference compound **1**. Interference *either* with the side lobes of the axial ligands (e.g. the C_A signature of species **4**) *or* with multiple scattering paths (e.g. the C_B signature of species **3**) results in more or less severe amplitude distortions.

two chlorine atoms,[45] which contrasts with the trans configuration found in both porphyrin complexes **2** and **4**. The factors governing cis versus trans coordination geometries in macrocyclic titanium(IV) complexes have been analyzed and discussed by Goedken et al.[45]

3.3. X-ray Absorption Spectra. 3.3.1. Dihalogenotitanium(IV) Porphyrin Complexes. The FT Im$[\tilde{\chi}_{(2):1(R)}]$ spectra of the dihalogenotitanium(IV) porphyrin complexes $[(TPP)Ti^{IV}X_2]$, i.e. species **2–4**, are compared in Figure 5. One should keep in mind that E_0 was carefully selected in order to let the signatures of the 4 N, 8 C_A, 4 C_{meso}, and 8 C_B atoms exhibit approximately the same phase.[14-18] It is, however, a feature common to all TPP complexes that the intensity of the $C_{1\varphi}$ carbon signature (i.e. the signature of the closest carbon atoms $C_{1\varphi}$ of the four phenyl meso substituents) is enhanced whereas its phase is nearly inverted;[46] this is a well-known consequence of the quasicollinear arrangement of the metal, the methine carbons C_{meso}, and the carbons $C_{1\varphi}$ which lead the contributions of multiple scattering paths (MS) to become dominant (e.g. the triple scattering path of the photoelectron: Ti $\rightarrow C_{meso} \rightarrow C_{1\varphi} \rightarrow C_{meso} \rightarrow$ Ti). Note that the assignment of the C_B signature is also somewhat ambiguous:[46] this signal peaks in all metalloporphyrin spectra at a distance that is systematically too short and thus prevents its assignment to a pure SS path.

It appears from Figure 5 that the signal of the axial ligands can interfere to a variable extent with the signal of the four equatorial nitrogen atoms. In the case of compound **2** (i.e. the difluoro complex), the interference between the EXAFS modulation of the two axial fluorine atoms and of the four equatorial ligands is so strong that the peak of the four nitrogen atoms simply vanishes, whereas the typical signatures of the carbons C_A, C_{meso}, C_B, and $C_{1\varphi}$ exhibit only minor amplitude distortions. This result is strongly reminiscent of a situation previously reported by Friant et al.[17] for the peroxotitanium(IV) porphyrinato complex $[(TPP)Ti^{IV}(O_2)]$. As regards the dichloro derivative, further complications arise from the difference in the scattering phase shifts of nitrogen and chlorine[23] and there is no way to localize the true position of the two chlorine atoms precisely from Figure 5.

The signatures of the Ti–C_β shells of species **1–4** are displayed with an expanded scale in Figure 6. While the metal is clearly shifted out from the porphyrin mean plane in the case of the oxotitanium(IV) compound **1**,[14,17,18] the shorter distances observed for complexes **2–4** indicate that the metal is most probably located in the porphyrin plane and support a trans configuration of the halogen atoms over the whole series **2–4** as confirmed by the crystal structures of complexes **2** and **4** or the ^{1}H NMR spectra taken from solutions. This comparison also suggests that there

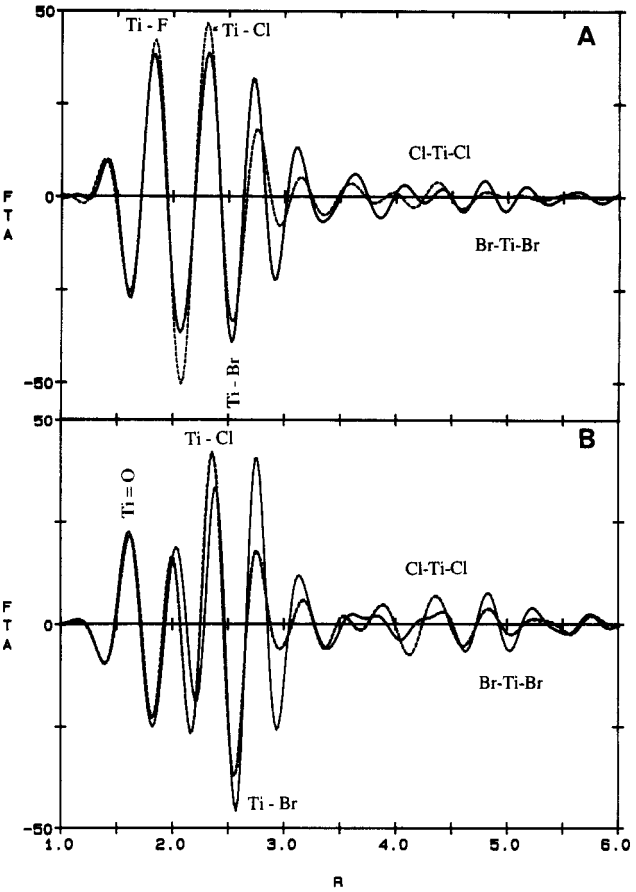

Figure 7. (A) Direct difference FT Im $[\tilde{\chi}_{(2):1}(R)]$ spectra: (—) $[(TPP)Ti^{IV}F_2] - [(TPP)Ti^{IV}Br_2]$; (---) $[(TPP)Ti^{IV}F_2] - [(TPP)Ti^{IV}Cl_2]$. (B) Perturbed difference FT spectra of the oxotitanium porphyrin **1** relaxing the combined effects of a reasonable axial shift (δh = 0.50 Å) and of a *small* doming (δ_{dom} = –0.08 Å) of the porphyrin core; (—) $[(TPP)Ti^{IV}{=}O] - [(TPP)Ti^{IV}Br_2]_{perturbed}$; (---) $[(TPP)Ti^{IV}{=}O] - [(TPP)Ti^{IV}Cl_2]_{perturbed}$.

should be no significant change in the radius of the macrocyclic cavity nor any distortion of the porphyrin planarity over the series **2–4**.

We thus expect the *direct* difference spectra reproduced in Figure 7A to be strongly dominated by the difference $\tilde{\chi}_{(2)}(Ti \rightarrow X \rightarrow Ti) - \tilde{\chi}_{(2)}(Ti \rightarrow Y \rightarrow Ti)$, where X and Y are the axial ligands of the species involved in the comparison. In practice,

(45) Goedken, V. L.; Dessy, G.; Ercolani, C.; Fares, V.; Gastaldi, L. *Inorg. Chem.* **1985**, *24*, 991–995.
(46) Goulon, J.; Goulon-Ginet, C.; Niedercorn, F.; Selve, C.; Castro, B. *Tetrahedron* **1981**, *37*, 3707–3712.

Table IX. Summary of the Major Parameters Deduced from the EXAFS Data Analyses Defining the Coordination of Titanium in Species **1–8**

species	R_{Ti^*-X}, Å	R_{Ti^*-N}, Å	R_{Ti^*-Ct}, Å	δh, Å	δ_{dom}, Å
1	1.62 ± 0.02	2.10 ● 0.02	2.04 ± 0.02	0.55 ● 0.05	$0.05_5 \pm 0.02_5$
2	1.80 ± 0.01	2.04 ± 0.02	2.04 ± 0.02		
3	2.32 ± 0.02	2.04 ± 0.02	2.04 ± 0.02		
4	2.45 ± 0.01	2.04 ± 0.02	2.04 ± 0.02		
5	1.95 ± 0.02	$2.11_5 \pm 0.02$	2.04 ± 0.02	0.64 ± 0.05	$0.08_0 \pm 0.02_5$
6	$2.41_6 \pm 0.01$	$2.11_5 \pm 0.02$	2.04 ± 0.02	0.64 ± 0.05	$0.08_0 \pm 0.02_5$
7	1.80 ± 0.02	2.11 ± 0.02	2.06 ± 0.02	0.50 ± 0.05	$0.05_5 \pm 0.02_5$
8	1.88 ± 0.03	2.04 ± 0.02	2.04 ± 0.02		

the readability of these difference spectra may appear somewhat confusing as a consequence of the different scattering phase shifts of the three halogen atoms (X = F; Y = Cl or Br). Nevertheless, we wish to emphasize the quite remarkable reproducibility of the Ti → F → Ti signature, which is now well resolved: the Ti–F peak positions (see Figure 7) differ by less than 0.01 Å. These difference spectra can alternatively be fitted in the momentum space by using a two-shell model: Figure S-1 (provided as supplementary material) gives a typical illustration of the nearly perfect agreement obtained in R space between real and simulated difference FT spectra. The refined interatomic distances summarized in Table IX are nicely consistent with the reference crystal structure data.

It was interesting to check how sensitive the difference analysis was to a contraction of the Ti–N distances by ca. 0.02 Å in complex **2** with respect to species **4**. Indeed Figure S-2 (also provided as supplementary material) produces direct evidence that such a contraction is most unlikely: when the experimental spectrum of species **4** is perturbed so as to simulate such a contraction, the signatures of the carbon C_A no longer cancel out in the FT difference spectrum and a large residual signal becomes immediately detectable. We therefore believe that *one should not retain as real* the small difference found in the single-crystal X-ray diffraction determination of the Ti–N bond lengths in species **2** and **4**.

It was also attractive to generate the artificial FT spectra of a "quasi-naked" porphyrin by subtracting from the real experimental spectra of species **2–4** the SS contributions of the axial ligands: as illustrated by Figure S-3 (supplementary material), the Ti–N signatures derived from the spectra of species **2** and **4** were found to be perfectly superimposed. A tentative refinement of the Ti–N signal by standard procedures (i.e. FT filtering plus fitting in momentum space) gave us R_{Ti-N} = 2.04 ± 0.02 Å depending on how E_0 is readjusted.

We wish to show that the oxotitanium complex **1** can be taken as a reference in difference analyses as well even though the metal is significantly shifted out from the porphyrin plane whereas some "doming" of the macrocycle is most probable. The best cancellation of the porphyrin signatures was achieved by combining a relatively large axial shift ($\delta h \simeq -0.5_0 \pm 0.0_5$ Å) of the metal back to the average porphyrin plane *with* a tiny doming correction of the porphyrin core ($\delta_{dom} \simeq -0.08 \pm 0.03$ Å); a simultaneous alteration of the diameter of the macrocyclic cavity was attempted but did not improve the quality of the difference spectra significantly, and thus it was abandoned (δd_{cav} = 0.00 Å). We do not claim that this is the unique solution because the three *perturbations* δh and (δd_{cav} and δ_{dom}) are implicitly correlated. This ambiguity is illustrated by Figure S-4, which compares the perturbed spectra associated with *two extreme solutions*:

$$\delta h = -0.5_0 \text{ Å} \quad \delta_{dom} = -0.0_8 \text{ Å} \quad \delta d_{cav} = -0.0_0 \text{ Å}$$

and

$$\delta h = -0.6_0 \text{ Å} \quad \delta_{dom} = -0.0_5 \text{ Å} \quad \delta d_{cav} = -0.0_4 \text{ Å}$$

Such small structural differences between two (perturbed) experimental spectra are shown to remain quite detectable, and such direct simulations can easily be used as a practical way to determine realistic limits for the correlated errors as a whole. Nevertheless, the order of magnitude of δh compares well with the known axial shift of the metal estimated from the crystal structure of another oxotitanium complex, [(OEP)Ti^{IV}=O] ($\delta h \simeq 0.60$ Å), whereas the latter compound also revealed a significant doming of the porphyrin core ($\delta_{dom} \simeq 0.05_5$ Å).[14,18] If the Ti–O bond length is to be determined, then it is more convenient to use the experimental spectrum of the dichloro complex **3** (or dibromo complex **4**) now as a reference and to simulate the inverse perturbation. The corresponding difference FT spectra are shown in Figure 7B. Again, one should notice the fair reproducibility of the Ti–O signal peaking at ca. $R = 1.6_2 \pm 0.0_2$ Å. The phase of the Ti–O signal is slightly distorted: this is partly due to the fact that the E_0 value was selected in the primary analysis as a compromise preserving the same phase for nearly all the signatures of the porphyrin pattern. A curved-wave formalism had also been preferable for the analysis of signals peaking at such short distances, but such an ultimate refinement was beyond the goals of the present study.[26]

One may suspect higher order correlations, e.g. the triple scattering paths Ti → X → Ti → X → Ti, to become detectable in difference analyses. Note that the trans configuration of the halogen atoms (with its *collinear* X–Ti–X sequence) is most conducive to the detection of these higher correlations, especially with heavy scatterers such as chlorine or bromine. Signatures peaking at nearly twice the Ti–X distance and featuring a distorted phase (with respect to the single scattering Ti → X → Ti signal) can be well identified in Figure 7B.

3.3.2. Cis-Disubstituted Titanium(IV) Porphyrin Complexes. (i) The Toluenedithiolato Complex [(TPP)Ti^{IV}(–S–)$_2$Tol] (6). The FT spectrum of species **6** confirmed that the metal was significantly shifted above the porphyrin mean plane, direct difference analyses being then totally hopeless. By trial and error, we found that it was still possible to produce a nearly perfect cancellation of the porphyrin pattern in difference spectra when the reference spectra were modified in order to simulate the following (self-consistent) structural perturbations:

for the titanyl complex **1**: $\delta h = +0.1_4$ Å, $\delta_{dom} = -0.0_0$ Å, $\delta d_{cav} = -0.0_0$ Å

for the difluoro complex **2**: $\delta h = +0.6_4$ Å, $\delta_{dom} = +0.0_8$ Å, $\delta d_{cav} = +0.0_0$ Å

The FT Im [$\tilde{\chi}_{(2):1}(R)$] spectra of species **6** and of the "perturbed" references are displayed in Figure S-5 (supplementary material), whereas the corresponding difference FT spectra are shown in Figure 8. As expected, the difference spectrum is clearly dominated by the signature of two sulfur atoms peaking at $R_{Ti-S} \simeq 2.4_1 \pm 0.01$ Å. Note that for the sake of more clarity, we took the argument of the well-known difference between the backscattering phase shifts of sulfur and fluorine (which differ by ca. π) for reversing the sign of the difference in order to obtain positive peaks for both the Ti–F and Ti–S signatures. At this stage, it was again most efficient to refine the analysis of these signatures by fitting the perturbed difference spectrum in the momentum k space (with a readjusted E_0 value and appropriate phase shifts/amplitude parameters). Our final result (see Table IX) converged to the average Ti–S distance found in the single-crystal structures of [(η-C_5H_5)$_2$$Ti^{IV}$(–S–)$_2$Ph] and [($\eta$-$C_5H_5$)$_2$$Ti^{IV}$(–S–)$_2$(CH=CH)].[47,48]

One may still detect in Figure 8 a few additional (reproducible) signatures that seem to be independent of the nature of the

(47) Kutoglu, A. *Z. Anorg. Allg. Chem.* **1972**, *390*, 195–209.
(48) Kutoglu, A. *Acta Crystallogr.* **1973**, *B29*, 2891–2897.

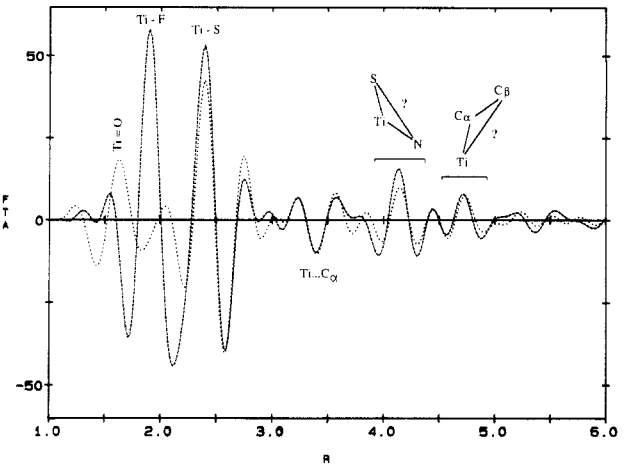

Figure 8. Perturbed difference FT Im $[\tilde{\chi}_{(2):1}(R)]$ spectra: (---) $-[(TPP)Ti^{IV}(-S-)_2Tol] + [(TPP)Ti^{IV}F_2]_{perturbed}$; (···) $-[(TPP)Ti^{IV}(-S-)_2Tol] + [(TPP)Ti^{IV}{=}O]_{perturbed}$.

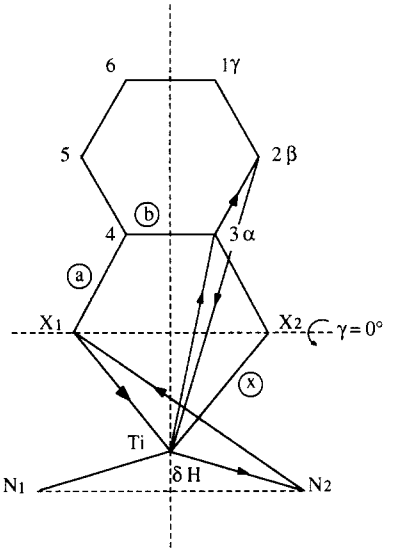

Figure 9. SS and MS paths contributing to the difference spectra in the cis-disubstituted derivatives: $x(5) = 1.95$ Å, $x(6) = 2.42$ Å; $a(5) = 1.35$ Å, $a(6) = 1.74_6$ Å; $b(5) = b(6) = 1.46$ Å. x values were derived from EXAFS spectra, whereas a and b were guesses extrapolated from crystal structure data.

compound selected as reference: their intensities are indeed much weaker when compared to the Ti–S signal, but their amplitudes are definitively above the statistical noise level of difference spectra. As their assignment remains perhaps ambiguous, the following discussion should be taken as tentative.

(i) At $R \simeq 3.4_0$ Å, one observes a (weak) negative signal: it may be asigned to the SS contribution of the two nearest α-carbon atoms (i.e. $C_{3\alpha}$ and $C_{4\alpha}$) of the toluene ring (see Figure 9). Its inverted phase would be consistent with this interpretation. If we assume that the toluenedithiol plane is folded out of the TiS_2 plane by the *same angle* (i.e. 46°) as in the aforementioned cyclopentadienyl complexes,[47,48] then the SS contributions of the α-carbon atoms should result in a negative peak at ca. $R \simeq 3.1_6$ Å. This value is too short when compared with the peak position found in our difference spectra; if there is no folding around the S_1S_2 axis, then the negative peak of the α-carbon atoms is precisely expected at ca. $R \simeq 3.4_1$ Å. It is therefore our interpretation that in complex **6** the folding angle is most probably small, the Ti–S–C bond angle falling in a more classical range (ca. 106° instead of 96° for the folded structures). The stereogeometry of complex **6** appears indeed much less propitious to allow similar interactions between a quasi-axial 3,4-toluenedithiolate ligand and the porphyrin macrocycle, as observed between the 3,4-toluenedithiolate ligand and the cyclopentadienyl ligands. It is also relevant to mention that small folding angles (e.g. γ = 5–9°) have been reported for several dithiolate chelates of molybdenum and tungsten.[48,49]

(ii) Additional arguments supporting the previous conclusion could be given if we were able to identify the signatures of the β-carbons (C_2 and C_5) of the toluene unit. The interatomic distance $Ti–C_{2\beta}$ is however strongly dependent upon the γ values e.g. $R = 4.77$ Å for $\gamma = 0°$ and $R = 4.44$ Å for $\gamma = 46°$, and vibrational disorder associated with the folding mode may prevent the detection of these weak signatures. Considering that the scattering angle between the two paths $Ti \rightarrow C_{3\alpha}$ and $C_{3\alpha} \rightarrow C_{2\beta}$ is on the order of 162° (if we assume $\gamma \simeq 0°$), interferences between SS and MS paths should be suspected. Nevertheless, there is a weak phase-inverted signal peaking at $R \simeq 4.7_0$ Å (see Figure 8) that might be (tentatively) assigned to the β-carbons. As far as this assignment is true, it would be most consistent with a small folding angle.

(iii) There is still a (stronger) signal peaking at ca. $R \simeq 4.1_5$ Å. It may be worth observing that its position, phase, and amplitude do not depend on the nature and stereogeometry of the compound selected as a reference (e.g. the fact that the metal is shifted out of the porphyrin plane in the oxotitanium complex **1** whereas it is located in the porphyrin plane in the case of the difluoro complex **2** does not make any strong difference). This led us to retain as most probable a tentative assignment of this signature to multiple scattering paths (MS) involving the sulfur atoms which are efficient scatterers: e.g. the double scattering paths $Ti \rightarrow N_i \rightarrow S_j \rightarrow Ti$ and the triple scattering paths $Ti \rightarrow N_i \rightarrow Ti \rightarrow S_j \rightarrow Ti$. We tried to simulate the latter contribution by assuming (for the sake of simplicity) that the two sulfur atoms S_1 and S_2 eclipsed the two equatorial nitrogen atoms N_1 and N_2 (see Figure 9): the simulation predicted a signal peaking very close ($4.1_8 \leq R \leq 4.3$ Å) to the signal of the difference spectrum.

(ii) The Catecholato Complex $[(TPP)Ti^{IV}(-O-)_2Ph]$ (5). Two major difficulties made direct differences again hopeless: (i) the metal is clearly shifted above the porphyrin mean plane; (ii) there appears to be a small reduction of the amplitude of the whole porphyrin pattern.

The first difficulty was cured by simulating a number of structural perturbations of the reference spectra. We rapidly came to the conclusion that the perturbations required for the difference analyses of complexes **5** and **6** were *the same* (within the limits of sensitivity of our difference analyses). Before addressing the second question concerning the amplitude reduction, we felt it essential to check for possible sources of experimental artifacts (e.g. poor sample quality and/or imperfect rejection of harmonics) that could cause similar effects. Luckily enough, this verification was negative: the rejection of harmonics by the two-mirror device could not be incriminated, and nothing special was detected about the homogeneity of the sample. Therefore, the observed effect had to be considered as real. In practice, we obtained a reasonable superimposition of the $Ti–C_A$ or $Ti–C_{meso}$ signatures (see Figure S-6 in the supplementary material for sample **5**) when the Debye–Waller factor was increased in eq 1 by the quantity $\Delta\sigma^2 = +0.001_5$ Å^2. A careful reinvestigation of the difference analyses carried out with species **6** revealed that a much smaller correction ($\Delta\sigma^2 \leq +0.000_8$ Å^2) could also reduce further the level of the residual difference signals without altering seriously our previous conclusions (in fact, this tiny Debye–Waller correction was included in the spectra shown in Figure 8). A possible origin for this amplitude effect will be discussed below.

The chelate structure of the catechol ligand is unambiguously confirmed by the difference FT spectra reproduced in Figure 10: these spectra are dominated by an intense Ti–O signal peaking at the rather long distance $R_{Ti-O} \simeq 1.9_5 \pm 0.0_2$ Å. The Ti–O bond length was again refined from a fit in the momentum k space, with use of the relevant phase shifts and a readjusted E_0 value. The final result ($R_{Ti-O} \simeq 1.9_5$ Å) is very close to the distance $R_{Cr-O} \simeq 1.9_8$ Å found in the crystal structure of the tris chelate $K_3Cr^{III}(catecholate)_3 \cdot 1.5H_2O$.[50] It differs significantly from the

(49) Debaerdemaeker, T.; Kutoglu, A. *Acta Crystallogr.* **1973**, *B29*, 2664–2668.

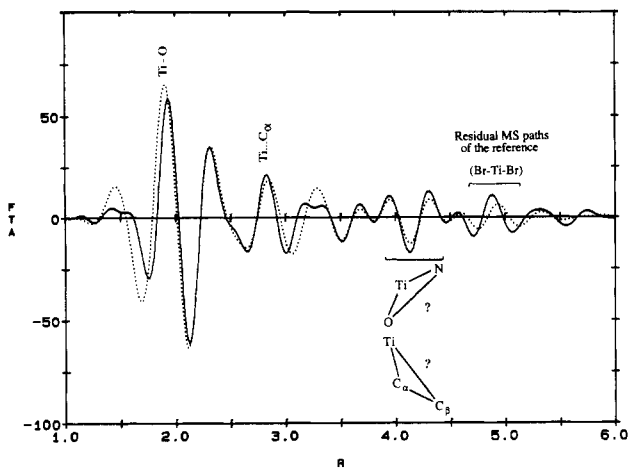

Figure 10. Perturbed difference FT Im $[\tilde{\chi}_{(2):1}(R)]$ spectra: (—) $[(TPP)Ti^{IV}(-O-)_2Ph]$ - $[(TPP)Ti(naked)]_{perturbed}$; (···) $[(TPP)Ti^{IV}(-O-)_2Ph]$ - $[(TPP)Ti^{IV}{=}O]_{perturbed}$.

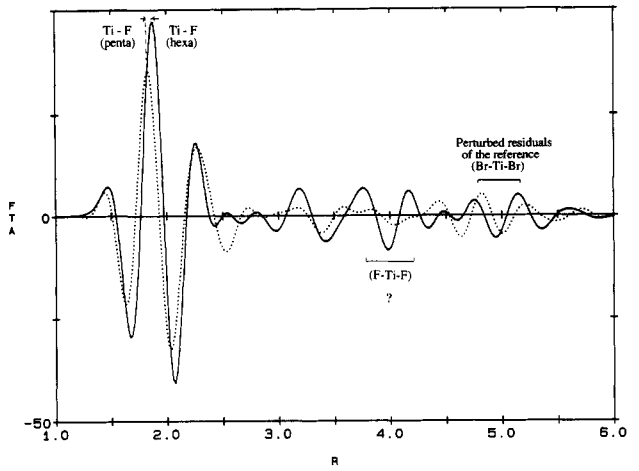

Figure 11. Perturbed difference FT Im $[\tilde{\chi}_{(2):1}(R)]$ spectra: (—) $[(TPP)Ti^{III}F_2]^-$ + [(TPP)Ti(naked)]; (···) $[(TPP)Ti^{III}F]$ - $[(TPP)Ti(naked)]_{perturbed}$.

Ti–O bond lengths $1.7_7 \leq R_{Ti-O} \leq 1.8_4$ Å classically accepted for monodentate axial ligation of titanium(IV) compounds.[2,7,17]

A *very tentative* assignment of the additional (residual) signatures of the difference spectra was attempted with the leading idea that some correlation with the interpretation proposed in the case of complex **6** might be found. Then, if we compare the difference spectra reproduced in Figures 10 and 8 (keeping in mind that the sign of the difference was inverted in Figure 8), it seems reasonable to assign the signal peaking at $R \simeq 2.8_1$ Å (and which is now positive) to the α-carbon atoms (i.e. $C_{3\alpha}$ and $C_{4\alpha}$). This assignment (if correct) implies that the folding angle around the O_1O_2 axis is (here also) very small (Figure 9). The assignment of the β-carbons is more ambiguous because the single scattering paths Ti → $C_{2/5\beta}$ → Ti, the double scattering paths Ti → $C_{3/4\alpha}$ → $C_{2/5\beta}$ → Ti, and the triple scattering paths Ti → $C_{3/4\alpha}$ → $C_{2/5\beta}$ → $C_{3/4\alpha}$ → Ti can interfere together with the triple scattering path Ti → N_i → Ti → O_j → Ti (see the discussion in the previous section): these various paths might contribute to the negative signal peaking at $R \simeq 4.13$ Å (see Figure 10).

On the other hand, it is our interpretation that the average amplitude reduction ($\Delta\sigma^2 = +0.001_5$ Å^2) may take its origin in the low barrier to hindered rotation of the chelating ligand around the symmetry axis of the porphyrin. The dioxygen adduct complexes $[(Por)Ti^{IV}(O_2)]$ are helpful models to discuss this point: dynamic NMR studies in solution made it clear that the barrier to rotation (or site exchange) of the dioxygen ligand was low (i.e. on the order of 10 kcal mol^{-1} [7]), the rotational motion being totally frozen out at low temperature, however. When performed on our complexes **5** and **6**, similar NMR investigations led to the conclusion that the barrier to rotation should be definitively lower because no splitting of the pyrrole proton resonances could be observed even when the solutions were cooled down to −180 °C.[19] We suspect that such a low barrier to rotation can affect the EXAFS spectra not only in solution but also in the solid state. In the crystal structure of $[(OEP)Ti^{IV}(O_2)]$, the presence of the dioxygen ligand reduces the symmetry from C_{4v} to C_{2v} and splits the characteristic interatomic distances of the porphyrin macrocycle into two series of unequal values, e.g. 2.0_9 and 2.1_3 Å for the Ti–N bond lengths, or 3.4_6 and 3.4_8 Å for the Ti–C_{meso} distances. Fast dynamic exchange between the eclipsed and noneclipsed configurations of the axial ligand could induce a structural disorder affecting the whole EXAFS pattern of the porphyrin macrocycle. In the solid state, even if the rotational motion is frozen out, some static disorder may still exist because of the broken C_{4v} symmetry whereas the low-frequency librational or torsional modes can add a substantial dynamic disorder when the barrier to internal rotation is low. Thus, if we accept this interpretation, our experiments might suggest that the barrier to hindered rotation is lower in the case of complex **5** as compared to that in complex **6**: this conclusion would be remarkably consistent with the results of our previous NMR studies.[19]

3.3.3. EXAFS Spectra of Titanium(III) Complexes. Only a few structural data are available on low-valent titanium(III) porphyrin complexes because these species are usually highly reactive and far less stable than titanium(IV) compounds.[2] Two questions can be raised: (i) Are there any significant changes in the Ti–F bond lengths between complexes **2**, **7**, and **8**? (ii) Can we learn anything about the localization (delocalization) of the additional charge on the metal?

There is a well-known correlation between the edge shifts and the charge localized on the absorbing atom (Kunzl's law),[51] but this correlation can be lost through concomitant structural modifications.[52,53] Therefore, it is essential to check with EXAFS spectroscopy for possible structural distortion before one can seriously address the question of the charge localization. Unfortunately, the phase shifts are also sensitive to variations of the charge localized on the absorber, the corresponding effects being often compensated by a small (artificial) shift of E_0. Difference FT analyses are obviously more sensitive than conventional analyses to such a shift of E_0, and we found that a negative shift, $\Delta E_0 \simeq -1.5$ eV, in the analysis of complex **8** let the signatures of the carbon atoms (C_A, C_{meso}, ...) become perfectly superimposed in the FT spectra of the two difluoro complexes **2** and **8** (see Figure S-7, supplementary material). We were further encouraged by the fact that the same shift (i.e. $\Delta E_0 \simeq -1.5$ eV) gave also the best results in the difference analyses of species **7**. It might be also relevant to indicate here that this energy shift would let the weak pre-edge structures A_{1g} be well superimposed in the first-derivative XANES spectra of compounds **2** and **8**.

The FT spectra of species **2** and **8** are compared in Figures S-7 and S-8 (supplementary material) and confirmed beyond any doubt that, in both cases, the metal was sitting in the porphyrin mean plane. *Direct* difference analyses were then well justified. For the sake of *more clarity*, we found it preferable to reproduce in Figure 11 one of the difference spectra obtained by subtracting from the unperturbed spectrum of species **8** the contribution of a quasi-naked porphyrin (i.e. the spectrum of species **4** after removal of the fitted SS contribution of the axial bromine atoms, just as described in section 3.3.1 and Figure S-3). The difference

(50) Raymond, K. N.; Isied, S. S.; Brown, L. D.; Fronczek, F. R.; Nibert, J. H. *J. Am. Chem. Soc.* **1976**, *98*, 1767–1774.

(51) Wong, J.; Lytle, F. W.; Messmer, R. P.; Maylotte, D. H. *Phys. Rev.* **1984**, *B30*, 5596–5610.

(52) (a) Natoli, C. R. In *EXAFS and Near Edge Structure II*; Bianconi, A., Incoccia, L., Stipcich, S., Eds.; Springer Series in Chemical Physics 27; Springer-Verlag: West Berlin, 1983; pp 43–56. (b) Natoli, C. R. In *EXAFS and Near Edge Structure III*; Hodgson, K., Hedman, B., Penner-Hahn, J. E., Eds.; Springer Proceedings in Physics 2; Springer-Verlag: West Berlin, 1984; pp 38–42.

(53) Bianconi, A.; Dell'Ariccia, M.; Durham, P. J.; Pendry, J. B. *Phys. Rev.* **1982**, *B26*, 6502–6508.

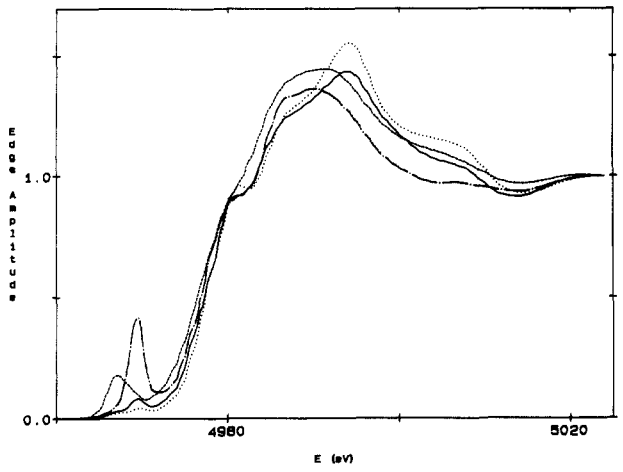

Figure 12. Comparison of the normalized XANES spectra of (—) [(TPP)$Ti^{IV}Br_2$] (**4**), (···) [(TPP)$Ti^{IV}Cl_2$] (**3**), (- - -) [(TPP)$Ti^{III}F$] (**7**), and (·–·) [(TPP)Ti^{IV}=O] (**1**).

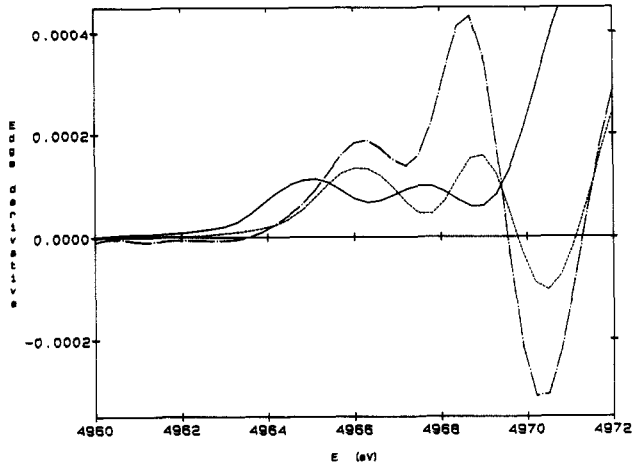

Figure 13. Expanded-scale plot of the first-derivative XANES spectra in the pre-edge region of (—) [(TPP)$Ti^{III}F_2$]$^-$ (**8**), (- - -) [(TPP)$Ti^{IV}Cl_2$] (**3**), and (·–·) [(TPP)$Ti^{IV}Br_2$] (**4**).

spectrum is then dominated by the strong signal of the two axial fluorine ligands (at $R_{Ti-F}(8) = 1.8_8 \pm 0.0_3$ Å), whereas the level of residual signatures *is very low*. A careful statistical analysis of these residual signatures indicated that it was not a pure white noise and we detected the contributions of well-identified multiple scattering paths (MS): Ti → X → Ti → X → Ti. Note that the spectrum of species **4** was preferred here for use as a reference because, even if the removal of the Ti–Br signatures is not rigourously perfect, their residual cannot interfere with the Ti–F signal, which peaks at a much shorter distance.

In the pentacoordinated species **7**, the metal is typically (see Figure S-8) shifted above the porphyrin mean plane, but to a lesser extent than in the titanyl complex **1**, and we found that the best cancellation of the whole porphyrin pattern occurred when **1** (the titanyl complex) was selected as reference with the perturbation $\delta h = -0.0_5$ Å and $\delta_{do}m = \delta d_{cav} = 0.0_0$ Å. Nevertheless, for more clarity and in order to be most self-consistent when comparing the Ti–F signatures of species **7** and **8**, we preferred to reproduce in Figure 11 the difference spectrum obtained with a *perturbed* quasi-naked porphyrin (using again as a reference the experimental spectrum of the dibromo derivative **4**). The advantage of such a choice is that the Ti–F signature is totally free of any interference with the perturbing Ti–O signal of complex **1**, whereas the residuals of the Ti–Br signals (if any) are to be found at much larger distances. The comparison of the difference spectra of species **2**, **7**, and **8** revealed that in the pentacoordinate complex **7** the Ti–F bond length is the same as in the difluorotitanium(IV) porphyrin complex **2**, the Ti–N bond lengths being slightly elongated due to the axial shift of the metal above the porphyrin mean plane. This elongation is quite consistent with the crystal structure data[44] of another five-coordinate Ti porphyrin (i.e. the methoxotitanium(III) porphyrin [(TPP)$Ti^{III}(OCH_3)$]), which shows long Ti–N bonds (average 2.12 Å). Note that, in the anionic species **8**, the situation is reversed; i.e., the Ti–N bond lengths remain unchanged (the metal being in the porphyrin mean plane), whereas the axial Ti–F bond lengths are significantly elongated ($R_{Ti-F}(8) = 1.8_8 \pm 0.0_3$ Å versus $R_{Ti-F}(2) = 1.8_0 \pm 0.0_2$ Å).

3.3.4. XANES and Pre-Edge Structures. We have reproduced in Figure 12 the normalized K-edge XANES spectra of complexes **1**, **3**, **4**, and **7**, whereas the first derivatives of the pre-edge structures of species **3**, **4**, and **8** are detailed in Figure 13. The XANES spectrum of the titanyl complex exhibits a strong prepeak associated with the C_{4v} symmetry allowed (1s → E or A_1) electric dipole transitions.[39,54] This prepeak has only half the intensity of the prepeak currently obtained with the related vanadium(IV) complex [(TPP)V^{IV}=O].[39,54] Part of this puzzling effect may certainly result from the modest energy resolution of the present experimental spectra, but this is not enough to account for the observed difference. INDO-S calculations revealed that, as regards the lowest antibonding states of symmetry E, the mixing between the metal ($3d_{xz}$, $3d_{yz}$) and oxygen ($2p_x$, $2p_y$) atomic orbitals should be more advantageous in the case of vanadium (the coefficients of the oxygen orbitals being ca. 10–15% higher). The prediction was not so clear for the A_1 state, where the possible mixing between the metal $3d_{z^2}$ and $4p_z$ atomic orbitals could be more important.

As regards the dihalogeno complexes **2**–**4**, the pre-edge structures are extremely weak, as expected for systems featuring the D_{4h} symmetry. As observed in other pseudooctahedral complexes,[55-58] the weak pre-edge structure exhibits a well-resolved doublet associated with forbidden transitions to the t_{2g} and e_g antibonding states (classically split by $\Delta E = 10Dq$): from the derivative spectra (Figure 13) we measured an approximate energy splitting of ca. 2.2 eV, which is only slightly lower than the 2.3–3.0 eV reported by Grunes[57] for rutile or anatase. According to the classical correlation table of the O_h group, a tetragonal distortion of the crystal field, resulting in a D_{4h} symmetry, would split the triply degenerate t_{2g} level in [B_{2g} + E_g] sublevels and the doubly degenerate state e_g in [A_{1g} + B_{1g}] substates, the corresponding energy differences being well below the natural width of the Ti K level (i.e. 0.94 eV). It seems that the contribution of the 1s → [A_{1g} + B_{1g}] transition increases significantly along the series **2** < **3** < **4**, whereas there is no similar effect for the 1s → [B_{2g} + E_g] transitions. Both sets of transitions are clearly quadrupole allowed, but we have no fundamental argument that enables us to predict any selective influence of the axial ligand on the transition intensities. Similarly, it is easy to check that both the 1s → A_{1g} and the 1s → E_g electric dipole transitions become allowed for the respective polarizations $\mu_z(A_{2u})$ and $\mu_{x,z}(E_u)$ when associated with the *same* (antisymmetrical) axial stretching mode of A_{2u} symmetry type.

The XANES spectrum of the five-coordinate titanium(III) complex **7** exhibits a broad pre-edge structure that is consistent with the C_{4v} molecular group symmetry; this prepeak is shifted toward lower energies by ca. 2.2 eV with respect to the corresponding structure of the titanyl complex **1**. In order to gain a deeper insight into the origin of this signature, INDO/S calculations were carried out on complex **7**, taking the structural data derived from EXAFS spectroscopy as first guesses. The energy diagram of the molecular orbitals confirmed that the highest occupied orbital was an α-spin B_2 state, with a dominant contribution of the Ti($3d_{xy}$) atomic orbital (95.0%) but no contribution from the axial ligand. As regards the lowest unoccupied states

(54) Penner-Hahn, J. E.; Benfatto, M.; Hedman, B.; Takahashi, T.; Doniach, S. *Inorg. Chem.* **1986**, *25*, 2255–2259.
(55) Shulman, R. G.; Yafet, Y.; Eisenberger, P.; Blumberg, W. E. *Proc. Natl. Acad. Sci. U.S.A.* **1976**, *73*, 1384–1388.
(56) Greegor, R. B.; Lytle, F. W.; Sandstrom, D. R.; Wong, J.; Schultz, P. *J. Non-Cryst. Solids* **1983**, *55*, 27–43.
(57) Grunes, L. A. *Phys. Rev.* **1983**, *B27*, 2111–2131.
(58) Petiau, J.; Calas, G. *Solid State Commun.* **1983**, *48*, 625–629.

we found (i) additional antibonding E states of the porphyrin ligand with a poor contribution of the metal $3d_{xz,yz}$ AO (less than 4.4%), (ii) α-spin and β-spin E states mixing the metal $3d_{xz,yz}$ AO (40%), the fluorine $2p_{x,y}$ AO (1.5%), and very diffuse contributions of the porphyrin ligand, and (iii) the α-spin and β-spin A_1 states mixing the metal $3d_{z^2}$ and $4p_z$ AO (52% and 23%), the fluorine $2p_z$ AO (5.5%), and again very diffuse contributions of the porphyrin ligand.

In our experience, the $3d_{z^2}$ and $4p_z$ AO mixing in the A_1 state is certainly very overestimated by INDO/S calculations. The core hole (not taken into account by ground-state INDO/S calculations) was shown to stabilize the antibonding orbitals E and A_1 by approximately the same amount (ca. 0.5 eV).[38] The energy splitting between the antibonding states E and A_1 of the titanyl complex **1** was found to be rather small (ca. 0.2 eV), but it was predicted to increase for complex **7** (up to ca. 0.6 eV): this could explain why the prepeak, which is very sharp in the XANES spectrum of the titanyl complex **1**, becomes so broad in the case of complex **7**. We observed also that the antibonding states of compound **7** were stabilized (by ca. −1.2 eV for the α-spin orbitals and −0.9 eV for the β-spin orbitals): this is *qualitatively* consistent with a shift of the prepeak toward lower energy, but the observed effect is twice as large as predicted by our (crude) theoretical calculation. From the trace of the INDO/S density matrix, one may still obtain a first estimation of the charge at the titanium atom: we found that in the low-valent species the net charge was reduced in a proportion of ca. 20%.

A comparison of the XANES spectra of *all* dihalogeno complexes does not reveal any significant shift of the absorption threshold (i.e. of the main peak in the first-derivative spectrum of the absorption edge: see Figure S-9 in the supplementary material), but the weak pre-edge structures of the anionic species **8** are slightly shifted toward lower energies ($\Delta E \simeq -1.5$ eV). Since the forbidden $1s \rightarrow [A_{1g} + B_{1g}]$ transitions do not exhibit any marked sensitivity to the nature of the axial ligand X in the case of complexes **2–4**, the shift observed for the anionic species **8** might well reflect a true variation in the charge localized at the metal. It might also be consistent with the small E_0 shift ($\Delta E_0 \simeq -1.5$ eV) that was required in the EXAFS data analysis of complex **8**.

4. Conclusion

The present paper discussed the spectrochemical and electrochemical properties of several titanium(IV)/titanium(III) porphyrin complexes. Structural information on these compounds was gained from EXAFS and X-ray crystallography.

(i) For the *trans*-dihalogenotitanium(IV) complexes, the Ti–X and Ti–N bond lengths were derived with an *absolute* uncertainty of 0.0_2 Å mostly due to imperfections in the phase-shift evaluation. The results are in excellent agreement with the crystal structure data. Note that the *relative* variations of the Ti–N interatomic distances along the series **2–4** were found to be less than 0.00_5 Å, i.e. well below the admitted limits of uncertainty of the crystal structure reported for complexes **2** and **4**.

(ii) For the cis-disubstituted titanium complexes **5** and **6**, as well as for the titanyl complex **1**, the perturbed difference FT analyses were most appropriate because the metal was found to be shifted out of the mean porphyrin plane. These analyses gave accurate determinations of the Ti–O and Ti–S bond lengths and led to reasonable estimations for the axial shift of the metal. Arguments were found which suggest that there is no significant folding of the catecholate or toluenedithiolate ligands around the O_1O_2 or S_1S_2 axes. Finally, we found that, in the case of the catecholate complex **5**, the porphyrin pattern was subject to some disorder: this might be explained by the extremely low barrier to internal rotation of the catechol ligand.

(iii) Difference analyses also confirmed that the metal was shifted out of the mean porphyrin plane ($\delta h \simeq 0.4_5 \pm 0.0_5$ Å) in the five-coordinate titanium(III) porphyrin complex **7**, whereas it lies in the porphyrin mean plane in the case of the six-coordinate anionic species **8**. In the latter compound the Ti–F distance ($1.8_8 \pm 0.0_3$ Å) is slightly longer than in the five-coordinate species **7** ($1.8_0 \pm 0.0_2$ Å). Charge delocalization was discussed with reference to the observed pre-edge structures.

Further work is still in progress in order to refine the error analyses and extract quantitative information from MS signals.

Acknowledgment. We are indebted to Dr. M. F. Ruiz-Lopez (University of Nancy-I) for his help in running INDO/S calculations.

Appendix

As shown below, errors can be estimated in difference EXAFS analyses with nearly the same level of validity (or limitation!) as for standard fits. The entropy S contained in a difference FT spectrum can be related to its power spectrum $P_S(R) = |\tilde{\chi}(R)|$ by using either one of the popular expressions

$$S = [2(\Delta B)]^{-1} \int_{R_{min}}^{R_{max}} \ln [P_S(R)]\, dR \quad \text{(Burg)} \qquad \text{(A1)}$$

$$S = [2(\Delta B)]^{-1} \int_{R_{min}}^{R_{max}} -P_S(R) \ln [P_S(R)]\, dR \quad \text{(Shannon–Jaynes)} \qquad \text{(A2)}$$

where: $\Delta B = R_{max} - R_{min}$ is the R-space spectral bandwidth subject to the Nyquist–Shannon sampling rate $R_{max} \leq 1/[2(\delta k)]$. On the other hand, the statistical (random) noise N can be evaluated from identical expressions, when the noise power spectrum $P_N(R)$ is substituted for $P_S(R)$. According to the Wiener–Khinchin theorem, $P_N(R)$ is simply the FT of the noise autocorrelation function measured in the k space for each data point j: $\langle \Delta\sigma_j(0) | \Delta\sigma_j(k) \rangle$ (which may be estimated, for instance, from a blank sample). It is possible to assess whether the cancellation of the signatures of the porphyrin macrocycle is good enough by checking whether the standard criterion $S/N \leq 1$ is (or is not) satisfied, S and N being evaluated here over a restricted bandpass (e.g. the R-space domain where the signatures of the carbon atoms C_A, C_{meso}, ... are expected to show up).

In perturbed difference analyses, we clearly assume that a porphyrin complex can be described with some crude structural model requiring p parameters. The same situation holds true obviously for conventional fits, and we propose to follow the same strategy, which is to reduce the information content in the proportion $\rho = [N_{pts} - p]/N_{pts}$, where N_{pts} ($=2(\Delta k)(\Delta B)/\pi$) is the number of independent data points in the experimental window $\Delta k = k_{max} - k_{min}$ for a given R-space band-pass ΔB.

Note that it may be difficult to take properly into account nonrandom noise (e.g. systematic errors), but the same objections can be raised against conventional fits.

Registry No. **1**, 58384-89-7; **2**, 66350-84-3; **3**, 66350-83-2; **4**, 66350-82-1; **5**, 92360-83-3; **6**, 92363-82-2; **7**, 71454-15-4; **8**, 123622-93-5; (OEP)TiF_2, 119890-37-8; (OEP)$TiCl_2$, 123622-94-6; (OEP)$TiBr_2$, 123622-95-7; $[(TPP)TiF_2]^{3-}$, 123622-96-8; $[(TPP)TiF_2]^{2-}$, 123622-97-9; $[(TPP)TiF_2]^{+}$, 123622-98-0; $[(TPP)TiF_2]^{2+}$, 123622-99-1; $[(OEP)TiF_2]^{-}$, 71414-24-9; $[(OEP)TiF_2]^{+}$, 123623-00-7; $[(OEP)TiF_2]^{2+}$, 123623-01-8; (OEP)TiF, 71414-23-8; (TPP)TiF(THF), 71414-25-0; (TPP)TiF(py), 71414-26-1; (TPP)TiF(1-MeIm), 71414-27-2; (TPP)TiF(NMP), 71414-28-3; (TPP)TiF(PBu_3), 71414-29-4.

Supplementary Material Available: Table S-I, giving a full presentation of crystallographic data for $[(TPP)Ti^{IV}F_2]$ (**2**), Table S-II, listing thermal parameters, and Figures S-1–S-9, showing EXAFS and XANES spectra (11 pages); Table S-III, listing calculated and observed structure factors (5 pages). Ordering information is given on any current masthead page.